Geophysical Journal International

Geophys. J. Int. (2014) **198,** 495–503
Advance Access publication 2014 May 23
GJI Seismology

doi: 10.1093/gji/ggu150

Infrasound signals from the underground nuclear explosions of North Korea

Il-Young Che,[1] Junghyun Park,[2] Inho Kim,[1] Tae Sung Kim[1] and Hee-Il Lee[1]

[1] *Earthquake Research Center, Korea Institute of Geoscience and Mineral Resources, Daejeon, Korea. E-mail: che10@kigam.re.kr*
[2] *Roy M. Huffington Department of Earth Sciences, Southern Methodist University, Dallas, TX, USA*

Accepted 2014 April 23. Received 2014 March 29; in original form 2013 December 7

SUMMARY

We investigated the infrasound signals from seismic ground motions induced by North Korea's underground nuclear explosions, including the recent third explosion on 2013 February 12. For the third explosion, the epicentral infrasound signals were detected not only by three infrasound network stations (KSGAR, ULDAR and YAGAR) in South Korea but also by two nearby International Monitoring System infrasound stations, IS45 and IS30. The detectability of the signals was limited at stations located on the relatively east side of the epicentre, with large azimuth deviations due to very favourable atmospheric conditions for eastward propagation at stratospheric height in 2013. The stratospheric wind direction was the reverse of that when the second explosion was conducted in 2009 May. The source location of the epicentral infrasound with wave parameters determined at the multiple stations has an offset by about 16.6 km from the reference seismic location. It was possible to determine the infrasonic location with moderate accuracy by the correction of the azimuth deviation due to the eastward winds in the stratosphere. In addition to the epicentral infrasonic signals, diffracted infrasound signals were observed from the second underground nuclear explosion in 2009. The exceptional detectability of the diffracted infrasound was a consequence of the temporal formation of a thin atmospheric inversion layer over the ocean surface when the event occurred.

Key words: Earthquake source observations; Seismic monitoring and test-ban treaty verification; Earthquake interaction, forecasting, and prediction.

1 INTRODUCTION

A world-wide network of sixty infrasound monitoring stations is being established as a part of the International Monitoring System (IMS) of the Comprehensive Nuclear-Test-Ban Treaty (CTBT). These international monitoring stations, with an average spacing of about 2000 km between neighbouring stations, will be used to verify the treaty by detecting and locating one kiloton or greater atmospheric nuclear explosions located at any point on the globe (Christie & Campus 2010). Although the system was originally designed to characterize atmospheric nuclear explosions it has, additionally, extended the detection regime of infrasound technology to other indirect explosive sources; for example, infrasound signals from the seismic ground motions associated with earthquakes (Le Pichon *et al.* 2002, 2006; Arrowsmith *et al.* 2009).

In addition, regional scale networks that range from several hundreds to thousands of kilometres in aperture have been used for analysing infrasound signals from earthquakes (Arrowsmith *et al.* 2012), mining explosions (Arrowsmith *et al.* 2008) and surface explosions (Hedlin *et al.* 2012). Walker *et al.* (2011) also used the dense regional seismic networks (EarthScope's USArray Transportable Array) to locate and characterize sources in the western United States. Subsequent work by Park (2013) has produced a bulletin of infrasound detections and locations using data from a regional infrasound network in the western United States. The Korean seismo-acoustic arrays (stations) were also used to analyse infrasonic signals from the second North Korean nuclear test (Che *et al.* 2009) and the results including the 2013 nuclear test using these arrays will be described later in this paper.

Korea Institute of Geoscience and Mineral Resources (KIGAM), in cooperation with Southern Methodist University (SMU), operates an infrasound array network called the Korean Infrasound Network (KIN) which consists of eight permanent seismo-acoustic arrays in South Korea (Fig. 1). The arrays have 0.2–1 km apertures with 4–18 acoustic gauges, Chaparral Physics Model 2 microphones or Inter-Mountain Labs (IML) sensors, connected to wind-noise reduction systems using porous hoses (Stump *et al.* 2004). These arrays are typically seismo-acoustic arrays, consisting of colocated seismometers and acoustic sensors. Each array can observe both seismic and infrasonic signals, and independently determine the location of a seismic source as well as the wave parameters of an infrasound signal. Therefore, near surface events such as large scale industrial blasts that emit both seismic and acoustic energy can be identified by the arrays. Compared with the IMS infrasound network, this is a relatively dense regional network. The average interarray spacing of the network is about 220 km, making it

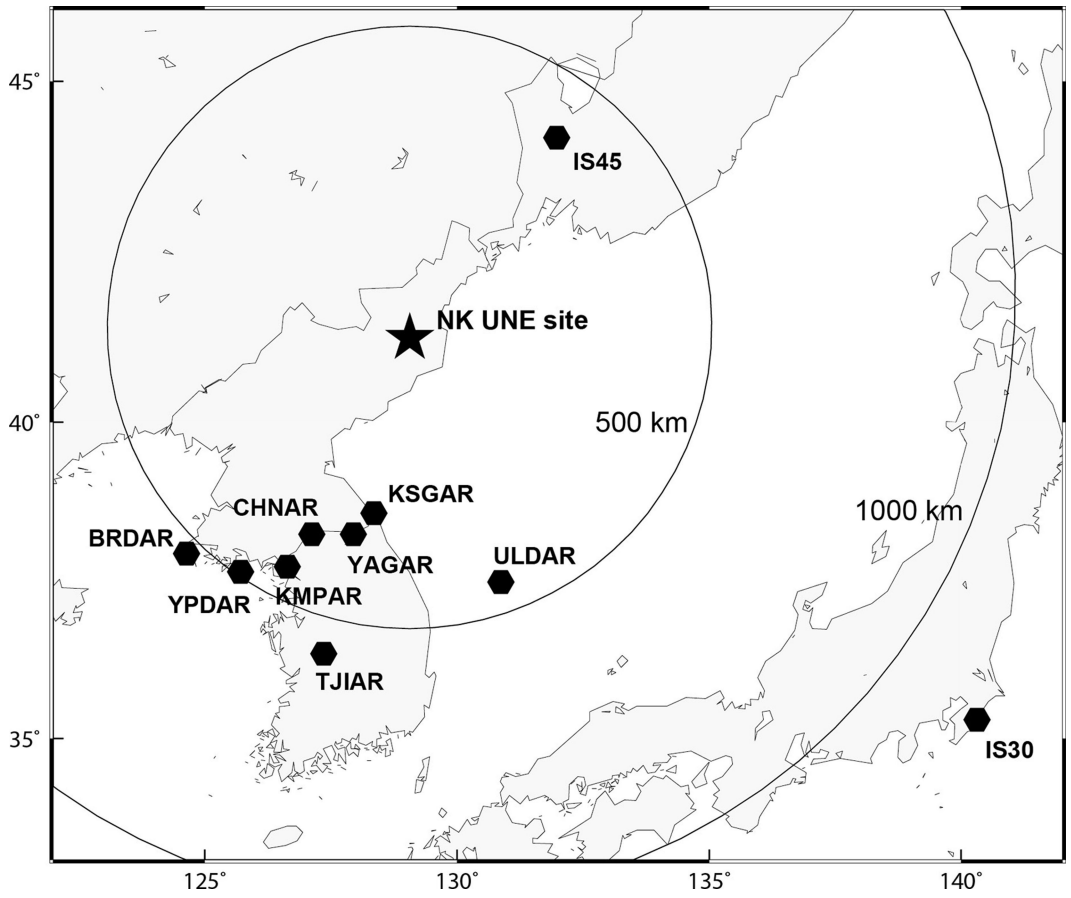

Figure 1. Location map of North Korea's underground nuclear explosion (NK UNE) site and eight infrasound stations of the KIN and two IMS stations (IS30 and IS45).

possible to detect small amplitude infrasound signals at multiple arrays and hence produce source locations with high accuracy at regional distances.

On 2013 February 12, North Korea conducted an underground nuclear test in the northeastern part of the Korean Peninsula. This was their third nuclear test after the two previous tests in 2006 and 2009. The infrasound signals associated with the 2009 explosion were observed at the five KIN arrays (Che *et al.* 2009). After the 2013 test, three seismo-acoustic arrays of the KIN and two nearby IMS stations recorded apparent infrasound signals from the explosion. The IMS stations are IS30 in Japan and IS45 in Russia have efficient wind-noise reducing system (consisting of pipe arrays) that is connected to the inlet of the infrasound sensor (Christie & Campus 2010) enhancing these observations.

The reference location of the third explosion determined by regional seismic data is almost collocated with those of the previous two explosions (Zhang & Wen 2013). The seismic magnitudes of the three sequential explosions were 3.9, 4.5 and 4.9 mb, respectively, indicative of increasing explosion yield (Chi *et al.* 2013). Although the depth of burial of each explosion is not known, it is generally accepted that all tests were conducted several hundred metres below the surface in a region of stable continental crust (Kim *et al.* 2009). Because no significant deformations have been reported on the surface after the explosions, the infrasound observed from the explosions could be interpreted as ground-to-air coupled waves due to the strong ground motions rather than the direct transfer of explosion energy to the atmosphere or deformational collapses at the epicentral area.

This study is the first assessment of the infrasound observations from the third underground explosion, and provides detection and location results for the event. The infrasound detection results of the three sequential underground explosions in North Korea, occurring in almost the same place with different yields, are compared alongside the prevailing atmospheric conditions. In addition, the infrasound source amplitudes are compared among the explosions. This study also describes the detection and location of diffracted infrasound signals from secondary sources by reviewing the data of the second explosion in 2009 and relating the event-dependent detectability with propagation conditions in the lower atmosphere.

2 EPICENTRAL INFRASOUND

An epicentral infrasound signal is caused by atmospheric pressure changes above the epicentral area of an earthquake and propagates through the atmosphere to remote ground-based infrasound stations. The mechanism of the generation of an epicentral infrasound signal is related to atmospheric pressure perturbations around epicentre. The atmospheric pressure change is generated by the pumping of the atmosphere by the strong ground motion around the source such as from Rayleigh waves from an earthquake (Arrowsmith *et al.* 2012). Since large-scale underground explosions also generate significant ground motions, infrasound generated from the site of an underground explosion can also be defined as epicentral infrasound.

While an epicentral infrasound signal is generated from the ground motions of either earthquakes or underground explosions, the differences in the source mechanisms of the point source of

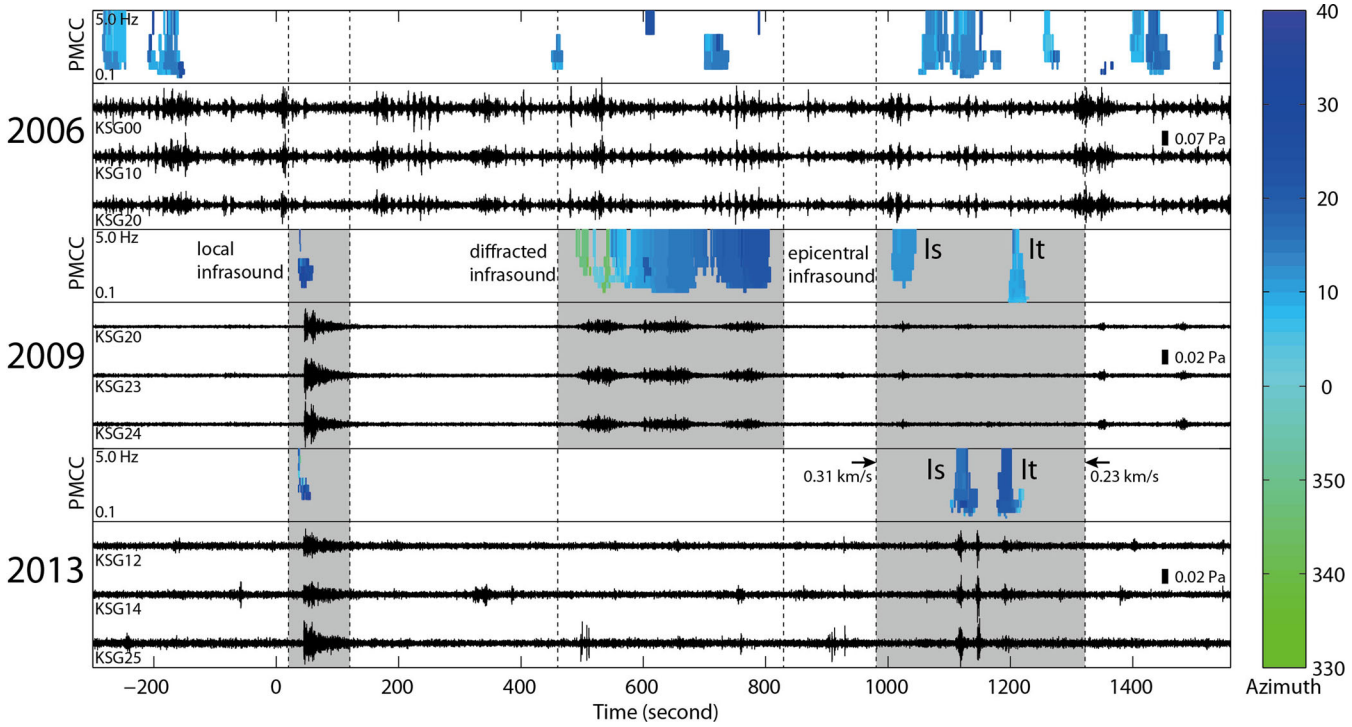

Figure 2. Waveforms and PMCC detection results for infrasound data recorded at KSGAR for three underground explosions in North Korea in 2006, 2009 and 2013. In each year, three sets of waveform data from KSGAR are plotted after band pass filtering between 2 and 7 Hz. All waveforms are aligned to seismic original time. Colours in the PMCC panels code the observed azimuth of detection at KSGAR. Only the PMCC detections from 330° to 40° are plotted. The true azimuth from KSGAR to the site is 11.3° from north. *Is* and *It* represent stratospheric and thermospheric infrasound arrivals, respectively. Local, diffracted and epicentral infrasounds in grey boxes indicate infrasound signals generated from different source locations; around receiver location, secondary source area and epicentral area, respectively.

explosions and the larger source area of earthquakes may result in waveform differences that are possibly distinguishable in terms of the infrasound signal's duration and amplitude with respect to the size of the seismic source. The longer duration of earthquake motion, as compared to the relatively short duration of an underground explosion, and the much larger amplitude of an underground explosion provides the potential to separate the two signal types (Whitaker 2007).

In 2009, five of seven seismo-acoustic arrays of the KIN detected the epicentral infrasound signals as well as seismic signals from the second underground explosion of North Korea (Che *et al.* 2009). In the third explosion in 2013, three stations (KSGAR, YAGAR and ULDAR) of the network detected a coherent epicentral infrasound signal. In addition to the Korean stations, two nearby IMS stations (IS30 and IS45) also detected the infrasound signals originating from the third explosion. Fig. 2 shows the infrasound waveforms of the three sequential underground explosions in North Korea, recorded at KSGAR (one of the Korean stations), which, at a distance of 304 km, was the closest station to the test site, and the results of the detection from the application of the progressive multichannel cross-correlation (PMCC) (Cansi 1995) to the waveforms in the frequency band of 0.1–5.0 Hz. The bottom panels show the results for the third explosion in 2013, where two impulsive infrasound signals were recorded ∼1114 and ∼1186 seconds after the seismic origin time with a celerity of 273 and 256 m s^{-1} and a predominantly high (∼2.7 Hz) and low (∼0.8 Hz) frequency, respectively. In a temperature-stratified atmosphere, Brown *et al.* (2002) documented several types of infrasound arrivals: tropospheric (referred to as *Iw*), stratospheric (referred to as *Is*) and thermospheric (referred to as *It*). An analysis of the 2009 observations (middle panel) identified two infrasound phases: a stratospheric (*Is*) and a thermospheric (*It*) arrival with a celerity of 302 and 254 m s^{-1} (Che *et al.* 2009). The second signal of the 2013 explosion has a similar celerity and frequency characteristics to that of the *It* phase of the 2009 explosion. The first signal preceding the apparent *It* phase of the 2013 explosion can be identified as the *Is* phase based on its celerity and higher frequency than the *It* phase. The discrepancy in the celerity of the *Is* phase between the 2009 and 2013 explosions could be explained by the systematic variation of travel time due to the seasonal temperature and wind effect along the path between 2009 May and 2013 February (Che *et al.* 2011). The faster stratospheric group velocity for 2009 in comparison to 2013 may reflect the higher temperatures in May relative to February (Fig. 2). In contrast, there is little difference in the celerity of *It* phases because the increasing thermal sound velocity at about 100 km altitude is sufficient to refract this phase throughout the year without seasonal variation (Whitaker & Mutschlecner 2008). The celerities of dominant phase at the other stations (YAGAR, ULDAR, IS45 and IS30) at distances of 347–1185 km were estimated to be between 275.8 and 309.7 m s^{-1}. The observed celerity values in Table 1 might have measurement error caused by picking onset time of infrasound signals. However this error is estimated to be less than 0.1 per cent of celerity because picking error is at most 1 second which is incomparably smaller than the traveltimes of the infrasound signals. In summary, the epicentral infrasound was predominantly propagated through the atmosphere as the *Is* phase trapped between the stratopause and the ground.

In 2006, five seismo-acoustic arrays of the KIN were being operated in South Korea and data for IS30 were available at that time. During the first explosion in 2006, only KSGAR detected a

Table 1. Parameters of observed and predicted infrasound signal (*Is*) at five stations.

Station	Distance (km)	True azimuth (°)	Observed azimuth with standard deviation (°)	Observed celerity (m s^{-1})	Predicted azimuth deviation (°)	Predicted celerity (m s^{-1})
KSGAR	304.0	11.3	15.8 ± 1.6	272.9	−3.6	290
YAGAR	347.0	15.6	21.1 ± 1.2	275.8	−4.4	280
IS45	403.2	217.3	211.6 ± 0.9	295.2	+3.1	310
ULDAR	445.3	340.1	343.8 ± 2.3	305.2	−4.0	305
IS30	1184.9	307.3	312.1 ± 0.4	309.7	−4.5	315

suspected infrasound signal, with the azimuth pointing towards the test site and an arrival time and group velocity consistent with possible epicentral infrasound (0.31–0.23 km s^{-1}), as shown in the upper panel of Fig. 2. However, infrasound signals with similar azimuths appeared at other times including the time period prior to the seismic arrival and extending for a long time following the explosion. Thus, the suspected signals were not positively identified as epicentral infrasound signals, and were classified as an unknown source, possibly located between the epicentre of the explosion and the station.

In addition to the epicentral infrasound signals, the figure showed detections of other types of infrasound signals, local and diffracted infrasound which will be discussed in section 3. Local infrasound occurs when seismic waves passing the array generate acoustic signals. At KSGAR, local infrasounds were clearly identified from the second and third explosion, indicative of larger ground motions than that of the first explosion.

Atmospheric ray tracing was performed to improve the assessment of the epicentral infrasound from the 2013 explosion and particularly assess the ability to predict wave parameters at the time of the explosion which were later used for infrasound source location. For the ray tracing (Virieux *et al.* 2004), we used the European Centre for Middle-range Weather Forecast (ECMWF, www.ecmwf.int) atmospheric model to construct effective sound velocity profiles from the source to each station. Fig. 3 shows an example of the ray tracing result from the test site (seismic reference location of the 2013 explosion) to KSGAR station. Rays were shot with take-off angles from 60° to nearly 90° from the vertical. From the calculations, the *Is* and *It* phases were predicted as arrivals from the explosion. For the *Is* phase, the predicted eigenray had a celerity of 290 m s^{-1} and an azimuth deviation of −3.6°. For the *It* phase, a celerity of 230 m s^{-1} and azimuth deviation of −9.1° were predicted. There was a discrepancy in celerity between observation and prediction with the ray tracing estimating an arrival time of one to two minutes early. The true azimuth from the KSGAR station to the source was 11.3° from north with observed azimuths for *Is* and *It* of 15.8° and 21.6°, respectively. Using the predicted azimuthal deviations to correct the observations the corrected azimuths were 12.2° and 12.5°, quite close to the true azimuth. This azimuth correction offers the opportunity for improved infrasound source locations relying on azimuth observations at multiple arrays. Celerity and azimuth deviations were also estimated from ray tracing for the other four stations including YAGAR, ULDAR, IS45 and IS30. Azimuth corrections at the other stations for the *Is* phase ranged from −4.5° to +3.1° depending on the direction of propagation to the stations. The celerity of the *Is* phase was in the range of 280–315 m s^{-1} (Table 1).

The source location of the epicentral infrasound signal was estimated based on a least-square method. In the location method (Nielsen 2007), observation equations were written with azimuths and arrival times to solve a set of three unknown parameters including source coordinates latitude, longitude and source origin time. An initial approximation for source coordinate and time was decided from a simple solution determined by azimuth intersection method. The best solution was attained by iterative least-square method with the linearized equations. In case of atmospheric velocity model, we used the predicted celerity from source area to each array (Table 1). Fig. 4 shows the source locations for the epicentral infrasound signals of the 2013 explosion detected by three stations of the KIN and two IMS stations. In the figure, the blue lines are the azimuth estimated at the arrays and deviate considerably from the true azimuth to the source. As noted, this azimuthal deviation is consistent with the prevailing eastward zonal wind at the time the explosion

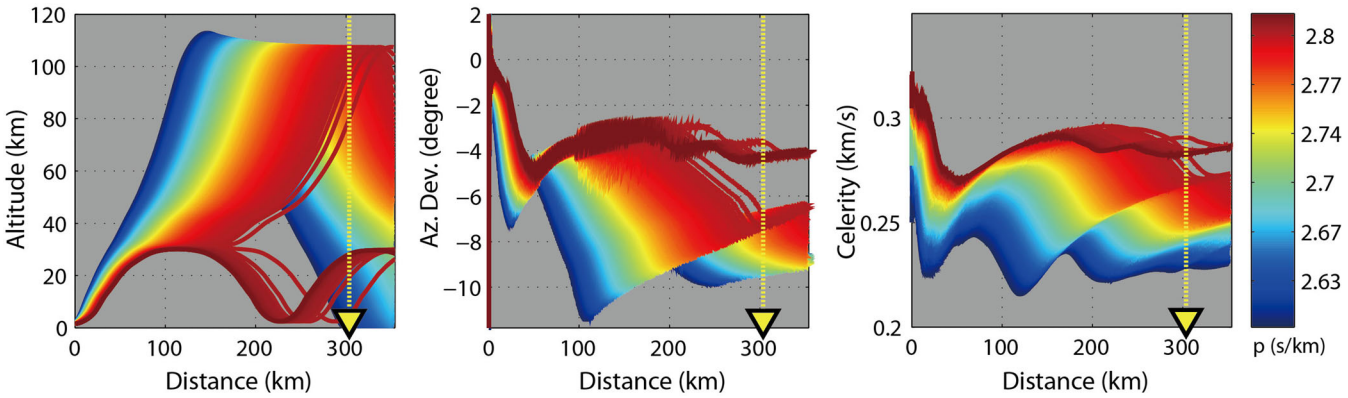

Figure 3. An example of the ray tracing results for propagations from the source to KSGAR (inverted triangle). Azimuth deviation and celerity were estimated from the nearest ray to the receiver. Colours indicate ray parameters (s km^{-1}).

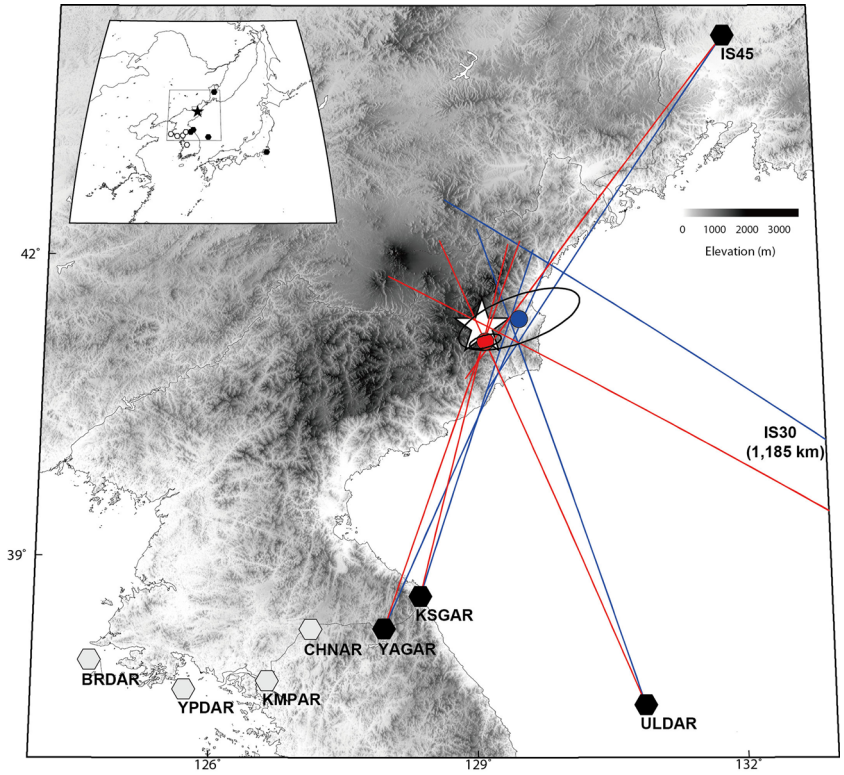

Figure 4. Source location results for the epicentral infrasound signal of the third underground explosion in North Korea. The blue circle denotes a location determined by using uncorrected azimuths (blue lines). Red lines are corrected azimuths based on ray tracing simulations, and the location determined by those azimuths is denoted by a red circle. The two ellipses indicate the 95 per cent confidence level of the event locations. The star and hexagons indicate seismic epicentre determined by regional seismic data and infrasound stations, respectively.

occurred. The blue circle in the figure is a location determined by the least-square method using the uncorrected azimuths and arrival times of detected signals. The red circle is the location of the epicentral infrasound using both the wind-corrected azimuth and the arrival times. As shown in the figure, the corrected azimuths were much closer to the reference seismic location after wind correction. The infrasonic location based on the wind-corrected azimuths and arrival times of the stratospheric phases was offset by about 16.6 km from the reference seismic location. This suggests that the wind correction for infrasound rays has improved the location result. The coincidence of the infrasound and seismic location is consistent with the signal interpretation as epicentral infrasound.

The stratospheric phase of the epicentral infrasound signal effectively propagates over long distances, controlled by the zonal wind in the stratosphere. The effective sound speed ratio ($V_{\text{eff-ratio}}$), defined as the ratio between the effective speed of sound at stratospheric altitudes and the speed of sound at ground level, is a proxy that can be used to describe atmospheric conditions explaining detectability in a given direction (Le Pichon *et al.* 2012). As an example of the detection results of the epicentral infrasound from the three explosions, the $V_{\text{eff-ratio}}$ was constructed at all altitudes in the atmosphere and azimuths using the ECMWF model. Fig. 5 shows the azimuthal variation of $V_{\text{eff-ratio}}$ profiles centred at the test site in 2006, 2009 and 2013, respectively. Warm colours ($V_{\text{eff-ratio}} > 1$) indicate

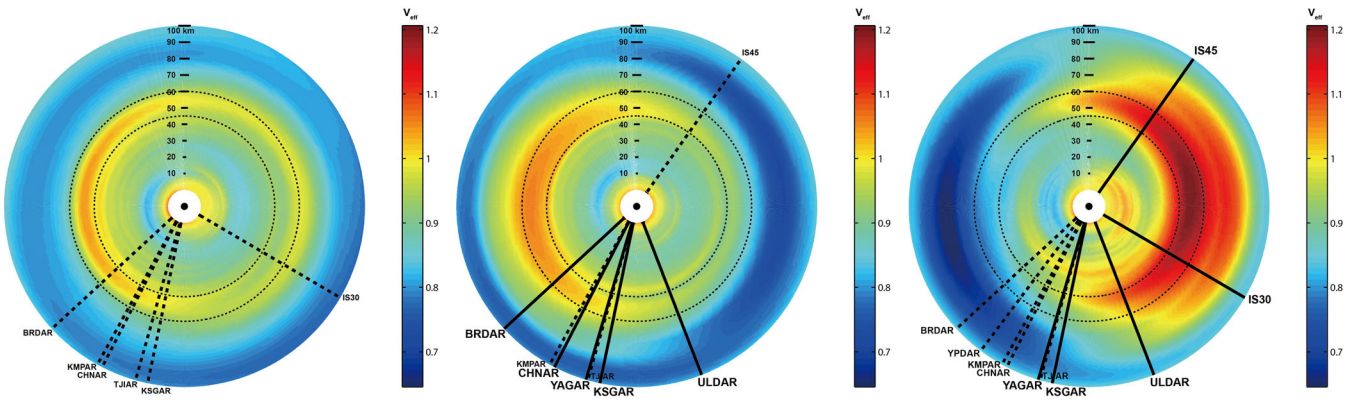

Figure 5. Azimuthal variation of $V_{\text{eff-ratio}}$ profiles centred at the North Korea test site for the 2006, 2009 and 2013 explosions. The colour scale represents the $V_{\text{eff-ratio}}$ determined from the ECMWF. Solid lines indicate azimuths from the source to stations that detected infrasonic signals; dotted lines for stations where no direct infrasound is detected.

Table 2. Comparisons of the infrasound amplitudes and the energies calculated at KSGAR station for the 2009 and 2013 explosions.

Explosion	Range (R, km)	Raw amplitude (P_{raw}, μbar)	Stratospheric wind velocity (V_s, m s^{-1})	Corrected amplitude (P_{wca}, μbar)	Charge weight (*chgwt*, ton)
2009	304	0.19	1.3	0.18	0.66
2013	304	0.68	4.4	0.57	3.39

favorable downwind propagation for a given azimuth, in which a ray can be trapped between a certain height and the ground. It shows that a westward wind, two inner circles between 30 and 50 km, prevailed in the stratosphere at the time of the 2006 and 2009 explosions. In contrast to the $V_{\text{eff-ratio}}$ of 2006 and 2009, the $V_{\text{eff-ratio}}$ of 2013 indicates favourable atmospheric conditions for eastward propagation. These atmospheric conditions are correlated with infrasound detectability at the stations in 2009 and 2013. In 2009, stations located to the SW of the test site were able to detect the epicentral infrasound due to the westward wind in the stratosphere. The detectability in 2013 was the opposite of 2009, with atmospheric conditions limiting the detectable azimuth range, that is, conditions were favourable for stations located on the relatively east side of the test site to record the infrasound signals. In addition, the atmospheric conditions with strong eastward zonal winds explain the large azimuth deviations at the stations. The eastward zonal wind accounted for differences in azimuthal deviation between stations with deviation to the right for IS45 and to the left for other stations.

For the infrasound signals detected from remote explosion sources, one important parameter that can be estimated from the signal is the energy released by the explosion. As the epicentral infrasound described above propagated through the stratospheric phase, an amplitude and energy relation, for example, as derived from the Los Alamos National Laboratory (LANL) high explosive (HE) test database (Whitaker *et al.* 2003; Evers *et al.* 2007), can be applied to the signals to calculate the energy released. However, although this is theoretically possible, the energy calculated for the epicentral infrasound of the North Korea's explosions cannot be regarded as the true explosion yield because the explosion energy was indirectly transferred to atmospheric acoustic energy by ground motions. It should be considered, rather, to be the energy equivalent of a HE explosion occurring on the surface. In this study we simply compare the relative amplitude of the epicentral infrasound between the 2009 and 2013 explosions, to assess the relative differences in ground motion between the two explosions. Based on the LANL wind correction that utilizes the observed amplitude (P_{raw}) and stratospheric wind (V_s) along the path from the source to the receiver, the wind corrected infrasound amplitude ($P_{wca} = P_{raw}10^{-0.018V_s}$) of the 2013 explosion was estimated to 0.57 μbar at KSGAR, which is about 3.2 times larger than the wind corrected amplitude of 0.18 μbar observed at KSGAR from the 2009 explosion (Table 2). In this study the V_s was estimated from average horizontal winds in the direction of propagation at the height of 25–35 km where the *Is* phase was refracted from ray tracing simulation in Fig. 3. The amplitude ratio is equivalent to an increase of a factor of 5.1 in terms of energy (*chgwt* in kilotons) released if the empirical relation is further applied, that is $P_{wca} = 59457(SR)^{-1.4072}$ where SR is the scaled range, $R/\sqrt{2 \times chgwt}$ and R is a range from the source to receiver in km.

3 DIFFRACTED INFRASOUND

A diffracted infrasound signal is often described as atmospheric acoustic signals generated by the interaction of the atmosphere with the movement of topographic features acting as secondary sources of acoustic energy. The most efficient source of diffracted infrasound is that of large earthquakes (Le Pichon *et al.* 2002; Arrowsmith *et al.* 2009). When earthquake-generated surface waves travel through high mountain regions between the epicentre and the receiver, the mountain areas can generate infrasound which arrives after the local infrasound and before the epicentral infrasound.

Diffracted infrasound was observed from the second underground explosion, as shown in middle panels of Fig. 2. The waveforms of the second explosion include diffracted infrasound as well as the epicentral infrasound. The arrival times of the diffracted infrasound which gradually commenced eight minutes after the seismic origin time were faster than that of epicentral infrasound. The arrival time order indicates the distance between the receiver and an inferred secondary source area at which the diffraction process occurred is shorter than the seismic epicentral distance. The five minutes duration of the diffracted infrasound indicates that the source areas were considerably larger than the area where the epicentral infrasound was generated. Observed azimuths at KSGAR varied clockwise from 342.0° to 27.2° with respect to the receiver. The amplitude of the signal was higher than that of epicentral infrasound, as described in the infrasound study of an earthquake in Nevada (Arrowsmith *et al.* 2009), indicating a relatively low attenuation during propagation.

The location of the area where the diffracted infrasound signal originated was estimated with a location inverse procedure incorporating ray tracing method to include azimuth deviation and celerity variation depending on source to receiver paths (Che *et al.* 2013). For the location of the diffracted infrasound signal, we first made an infrasound source map which covers a broad source area (a rectangular box in Fig. 6) to include all possible sources. At each grid node within the source map, azimuth deviation and celerity value were estimated from eigenrays that were predicted from ray tracing from the node to the receiver using the ECMWF atmospheric model. Thus, each node has its own possible infrasound travel time that includes both the propagation time of seismic wave and infrasound calculated from celerity at the node. To calculate seismic propagation time of peak ground motion to each node, the mean seismic velocity was estimated using epicentral distances and arrival times at regional seismic stations. The observed mean seismic velocity was ~3.3 km s^{-1}. Each node also has its own azimuth value that was corrected for azimuth deviation caused by the wind transverse to the direction of the eigenray. The best source location for each detection of the diffracted infrasound signal shown in the PMCC results of Fig. 2 were grid-searched from the infrasound source map in terms of infrasound arrival time and azimuth measured at the receiver (Che *et al.* 2013).

Fig. 6 shows source location results for the diffracted infrasonic signals based on the location procedure. The diffracted infrasound developed as secondary infrasound sources along approximately 180 km of the coastal area, as if the sources were moving along the coast in a SW–NE direction. According to the seismic velocity and the length of the coast line, the difference in the origin time between peak ground motions at the end of the coastal area is about half a minute. This indicates that the coastal areas almost simultaneously suffered ground motions after the explosion occurred.

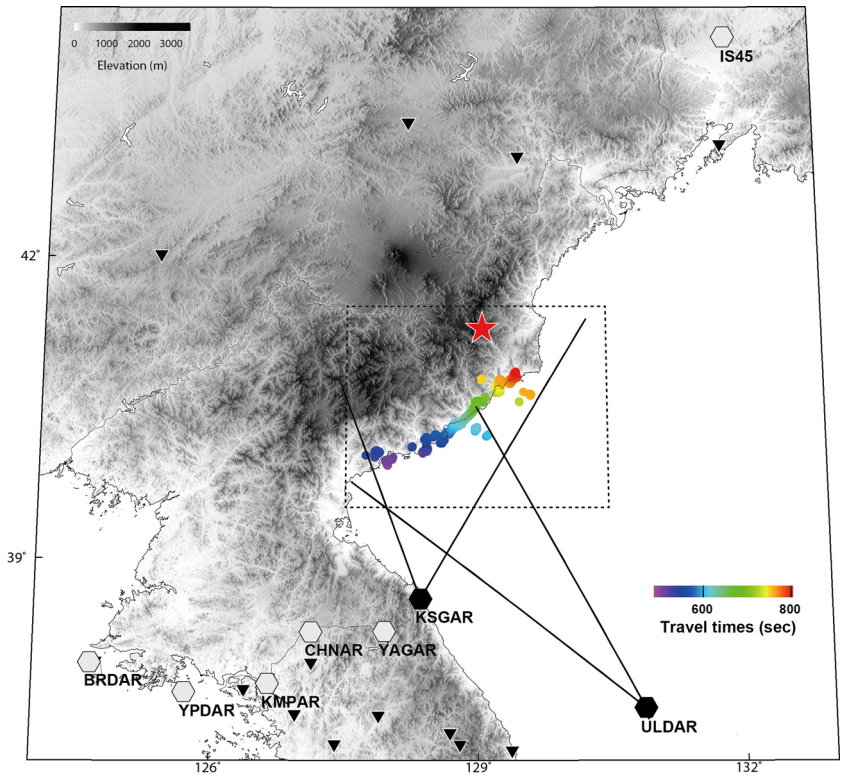

Figure 6. Source location of the diffracted infrasound signals based on a location inverse procedure. The dots indicate the resulting locations and their colour indicates the travel time after their seismic origin. Two lines from KSGAR and ULDAR indicate the observed azimuth range of the diffracted infrasound signals. Inverted triangles indicate the location of seismic stations from which data were used to measure the seismic velocity of peak ground motions.

Because the infrasound wave is about 10 times slower than the seismic surface wave, the different propagation distances from the coastal areas to the receiver increased the infrasound arrival time to about five minutes. Diffracted infrasound was observed at only two stations, KSGAR and ULDAR. ULDAR is located on an island and is exposed to an ocean environment, like the KSGAR station. The relative positions between the secondary sources along the coastline and receivers including KSGAR and ULDAR resulted in different signal characteristics in terms of arrival time and duration. Because the coastline has an oblique angle with respect to KSGAR, the infrasound signal from the southwest of the coastal area arrived first at KSGAR, and then the azimuths of the following signals rotated with time toward the northeast end of the coastal area. ULDAR is positioned almost perpendicular to the coast, thus the waveform is complicated by overlapping arrivals generated at different locations in the coastal area due to the locations having a similar distance to the sources. Azimuth ranges observed at ULDAR are also superimposed in Fig. 6.

The seismic location of the third underground explosion was almost the same as that of the second explosion and its seismic magnitude was larger than that of the second explosion (Zhang & Wen 2013). Therefore, a similar diffracted infrasound signal could be expected from the larger third explosion, because the diffraction process would have been induced at secondary source regions by the larger ground motions of the third underground explosion. However, it was not possible to detect the diffracted infrasound signals from the third explosion (Fig. 2).

This event-dependent detectability of the diffracted infrasound signal can be partly explained by atmospheric conditions. Fig. 7 shows a comparison of the spatial distribution of $V_{\text{eff-ratio}}$ at the elevation of 250 m above sea level and the effective sound velocity profiles in the lower atmosphere at the times of the 2009 and 2013 explosions. In the spatial distribution diagram, warm colours indicate a high $V_{\text{eff-ratio}}$ from various points to the receiver (KSGAR), indicating favourable propagation conditions in the lower atmosphere for the 2009 explosion.

In 2009 May, the $V_{\text{eff-ratio}}$ in the lower atmosphere indicated favourable conditions for wave propagation in the direction from the sources (the coastal areas) to KSGAR over the ocean. About 250 m above the ocean surface there was a speed of sound of up to 350 m s^{-1} in the SW direction that produced an energy duct for rays with higher take-off angles. In contrast, a normal velocity gradient was present in 2013 February, which resulted in acoustic energy diverging upwards. Thus, diffracted infrasound from the second explosion in 2009 was detectable due to an inversion layer in the lower atmosphere, over the ocean surface. The inversion layer might be related to the temporal variation of atmospheric structure in the near surface of the ocean. Morning in spring is often a time where an inversion layer forms over the ocean by the warm air moving over a cold ocean (Herrin *et al.* 2006). The ground-coupled acoustic wave could propagate over a long distance as guided waves in the inversion layer due to refraction caused by the temperature change at the boundary and reflection from the ocean surface.

The inversion layer pervaded the region around the KSGAR and ULDAR allowing infrasound generated by diffraction at the coastal area to propagate to large distance. YAGAR is located ∼50 km from KSGAR (Fig. 1). However, this station did not record the guided waves that propagated near the ocean surface. The guided waves were blocked from YAGAR by the mountain ranges between KSGAR and YAGAR with a height of 1 km above sea level.

The underground explosions would have resulted in maximum ground motions at the epicentral area with epicentral infrasound

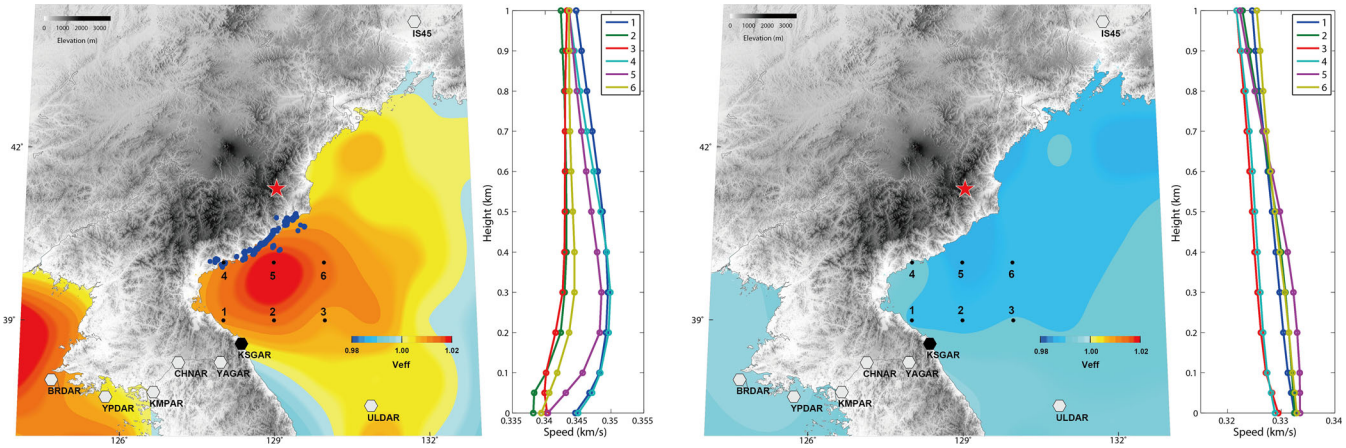

Figure 7. Spatial distribution of the $V_{\text{eff-ratio}}$ at 250 m above the ocean surface and effective speed of sound profiles at selected points over the ocean for the time periods of the 2009 (left-hand panel) and 2013 (right-hand panel) explosions. Blue dots on the left-side map are the source location results for the diffracted infrasound signals from Figure 6.

induced from the direct seismic energy transmission at the ground and atmosphere boundary. However, we could not observe any diffracted infrasound signals from the western part of the epicentre, which is a high mountain area. We conclude that atmospheric perturbations in the large mountainous area, except for the epicentre, did not propagate to the infrasound stations through the stratospheric phase due to unfavourable propagation conditions in the stratosphere. Only the diffracted infrasound from the coastal area, which is a marginal area of the mountain range that faces the ocean, was detectable at the ocean-side stations due to the thin acoustic duct layer that temporarily formed due to the specific conditions over the ocean surface.

4 CONCLUSION AND DISCUSSION

Three infrasound stations in South Korea and two IMS infrasound stations, IS30 in Japan and IS45 in Russia bordering North Korea, detected infrasound signals generated from the third underground nuclear explosion in North Korea on 2013 February 12. Compared with the 2006 and 2009 explosions, the strong eastward zonal wind in the stratosphere in winter altered infrasound propagation during the period when the 2013 explosion occurred. These atmospheric conditions made it possible to detect the infrasound signals at regional IMS stations located in the downwind direction. In addition, the strong wind resulted in large azimuthal deviations of arrivals at the observing stations. The infrasound source location based on arrival times and wind corrected azimuth of the stratospheric phase resulted in moderate location accuracy, which was comparable to the seismic locations. The observations from the two IMS stations are believed to represent the first detection of epicentral infrasound from underground nuclear tests after the adoption of the CTBT. Furthermore, the detection represents a validation of the extension of infrasound monitoring technology, originally focused on atmospheric explosions, to verify underground nuclear explosions by combining a subset of IMS stations and regional networks.

From the perspective of infrasound source discrimination, the observation of impulsive epicentral infrasound is possible evidence that the third seismic event, with a magnitude of 4.9, could be classified as a possible near surface explosion. Although ground motions caused by either a shallow earthquake or an underground explosion can generate infrasound signals observable at remote stations, the observations are consistent with the model that the short signal duration expected from an underground explosion due to the atmospheric coupling of the short-duration of strong *P* wave on the ground surface. As Whitaker (2007) has suggested, the differences in infrasound signals between underground nuclear explosions and earthquakes in terms of infrasound pressure amplitude versus seismic magnitude, and signal duration versus seismic magnitude, could be potential source discriminants.

The underground explosion series in North Korea produced unique infrasound signals of three types of coseismic pressure sources: local, epicentral and diffracted. In particular, the diffracted infrasound signal that has been reported mostly from larger earthquakes was observed from only the second explosion in 2009. The observation of the diffracted infrasound signal indicates that ground motions in secondary source regions are sufficient to generate infrasound signals. The source location results based on location inverse method were limited to the coastal area. This exceptional observation from only the coastal area for the 2009 explosion was likely to be due to favourable propagation conditions in the lower atmosphere over the ocean at the time of the explosion. A thin acoustic wave duct developed a low elevation over the ocean, thus only sources and receivers that were facing each other over the ocean were able to detect the signal. The detectability was also influenced by blockages between the waves and receivers as illustrated by the lack of a signal at YAGAR which is isolated by a 1 km high mountain range.

The infrasound source amplitude at the epicentre was estimated following correction for wind conditions along the path. The corrected amplitudes of the 2009 and 2013 explosion were 0.18 and 0.57 μbar, respectively at KSGAR which is the closest station. As the three explosions in North Korea are believed to have been conducted underground with an overburden of competent rocks, the explosive energy was not directly transferred to the atmosphere to generate the epicentral infrasound. Rather, the short time vibration of the ground by strong seismic waves from the explosions is considered to be the source of the infrasound signals, which were observed. Therefore, the wind corrected infrasound amplitude has a limitation in its use for calculating the true yield of the underground explosion. Rather, the amplitude ratio indicated that the peak ground motion of the third explosion was about three times larger than that of the second explosion in terms of the coupling relation (Donn

& Posmentier 1964) of the vertical ground motion velocity that is proportional to the air perturbation pressure.

ACKNOWLEDGEMENTS

The authors are grateful to the ECMWF for providing data for the atmospheric model and the Provisional Technical Secretariat (PTS) for providing the atmospheric model and infrasound waveform data from the IS30 and IS45 stations. We express our appreciation to Dr Brian Stump of Southern Methodist University for helpful comments. This work was supported by the Basic Research Project of the Korea Institute of Geoscience and Mineral Resources funded by the Ministry of Knowledge Economy of Korea.

REFERENCES

Arrowsmith, S.J., Hedlin, M.A.H., Stump, B. & Arrowsmith, M.D., 2008. Infrasonic Signals from Large Mining Explosions, *Bull. seism. Soc. Am.,* **98,** 768–777.

Arrowsmith, S.J., Burlacu, R., Whitaker, R. & Randall, G., 2009. A repeating secondary source of infrasound from the Wells, Nevada, earthquake sequence, *Geophys. Res. Lett.,* **36,** L11817, doi:10.1029/2009GL038363.

Arrowsmith, S.J., Burlacu, R., Pankow, K., Stump, B., Stead, R., Whitaker, R. & Hayward, C., 2012. A seismoacoustic study of the 2011 January 3 Circleville earthquake, *Geophys. J. Int.,* **189,** 1148–1158.

Brown, D.J., Katz, C.N., Le Bras, R., Flanagan, M.P., Wang, J. & Gault, A.K., 2002. Infrasonic signal detection and source location at the Prototype Data Centre, *Pure appl. Geophys.,* **159,** 1081–1125.

Cansi, Y., 1995. An automatic seismic event processing for detection and location: the PMCC method, *Geophys. Res. Lett.,* **22,** 1021–1024.

Che, I.-Y., Kim, T.S., Jeon, J.-S. & Lee, H.-I., 2009. Infrasound observation of the apparent North Korean nuclear test of 25 May 2009, *Geophys. Res. Lett.,* **36,** L22802, doi:10.1029/2009GL041017.

Che, I.-Y., Stump, B. & Lee, H.-I., 2011. Experimental Characterization of Seasonal Variations in Infrasonic Travel Times on the Korean Peninsula with Implications for Infrasound Event Location, *Geophys. J. Int.,* **185**(1), 190–200.

Che, I.-Y., Kim, G.Y. & Le Pichon, A., 2013. Infrasound associated with the deep *M* 7.3 northeastern China earthquake of June 28, 2002, *Earth Planets Space,* **65,** 109–113.

Chi, H.-C., Kim, G.Y., Shin, J.S., Kim, T.S. & Che, I.-Y., 2013. KIGAM evaluation of the 3rd NK nuclear test: comparison with the 1st and 2nd tests, in *Proceedings of the CTBT: Science and Technology 2013 Conference,* Vienna, Austria.

Christie, D.R. & Campus, P., 2010. The IMS infrasound network: design and establishment of infrasound stations, in *Infrasound Monitoring for Atmospheric Studies,* pp. 29–75, eds Le Pichon, A., Blanc, E. & Hauchecorne, A., Springer.

Donn, W.L. & Posmentier, E.S., 1964. Ground-coupled air waves from the great Alaskan earthquake, *J. geophys. Res.,* **69,** 5357– 5361.

Evers, L.G., Ceranna, L., Haak, H.W., Le Pichon, A. & Whitaker, R.W., 2007. A seismoacoustic analysis of the gas-pipeline explosion near Ghislenghien in Belgium, *Bull. seism. Soc. Am.,* **97,** 417–425.

Hedlin, M.A.H., de Groot-Hedlin, C. & Drob, D., 2012. A study of infrasound propagation using dense seismic network recordings of surface explosions, *Bull. seism. Soc. Am.,* **102,** 1927–1937.

Herrin, E.T., Kim, T.S. & Stump, B.W., 2006. Evidence for an infrasound waveguide, *Geophys. Res. Lett.,* **33,** L07815, doi:10.1029/2005GL025491.

Kim, T.S., Kang, I.-B. & Kim, G.-Y., 2009. Yield ratio estimates using regional Pn and Pg from North Korea's underground nuclear explosions, *Geophys. Res. Lett.,* **36,** L22302, doi:10.1029/2009GL040495.

Le Pichon, A., Guilbert, J., Vega, A., Garce´s, M. & Brachet, N., 2002. Ground-coupled air waves and diffracted infrasound from the Arequipa earthquake of June 23, 2001, *Geophys. Res. Lett.,* **29**(18), 1886, doi:10.1029/2002GL015052.

Le Pichon, A., Mialle, P., Guilbert, J. & Vergoz, J., 2006. Multistation infrasonic observations of the Chilean earthquake of 2005 June 13, *Geophys. J. Int.,* **167,** 838–844.

Le Pichon, A., Ceranna, L. & Vergoz, J., 2012. Incorporating numerical modeling into estimates of the detection capability of the IMS infrasound network, *J. geophys. Res.,* **117,** D05121, doi:10.1029/2011JD016670.

Nielsen, A., 2007. Least squares adjustment: linear and nonlinear weighted regression analysis. DTU Lecture Notes. Available at: www2.imm.dtu.dk/pubdb/views/publication_details.php?id=280410.1093/gji/ggu150.html (last accessed 16 April 2009).

Park, J., 2013. Infrasound signal processing from regional arrays and seismic characteristics of North Korean nuclear explosions, *PhD thesis,* Southern Methodist University, Dallas, USA.

Stump, B., Jun, M.-S., Hayward, C., Jeon, J.-S., Che, I.-Y., Thomason, K., House, S.M. & McKenna, J., 2004. Small-aperture seismo-acoustic arrays: design, implementation, and utilization, *Bull. seism. Soc. Am.,* **94,** 220–236.

Virieux, J., Garnier, N., Blanc, E. & Dessa, J.-X., 2004. Paraxial ray tracing for atmospheric wave propagation, *Geophys. Res. Lett.,* **31,** L20106, doi:10.1029/2004GL020514.

Walker, K.T., Shelby, R., Hedlin, M.A.H., de Groot-Hedlin, C. & Vernon, F., 2011. Western U.S. Infrasonic Catalog: illuminating infrasonic hot spots with the USArray, *J. geophys. Res.,* **116,** B12305, doi:10.1029/2011JB008579.

Whitaker, R.W., 2007. Infrasound signals as basis for event discriminants, in *Proceedings of the 29th Monitoring Research Review: Ground-Based Nuclear Explosion Monitoring Technologies,* pp. 905–913, Natl. Nucl. Secur. Admin., Washington, DC.

Whitaker, R.W., Sondoval, T.D. & Mutschlecner, J.P., 2003. Recent infrasound analysis, in *Proceedings of the 25th Seismic Res. Rev.—Nuclear Explosion Monitoring: Building the Knowledge Base,* pp. 646–654, Natl. Nucl. Secur. Admin., Tucson, Ariz.

Whitaker, R.W. & Mutschlecner, J.P., 2008. A comparison of infrasound signals refracted from stratospheric and thermospheric altitudes, *J. geophys. Res.,* **113,** D08117, doi:10.1029/2007JD008852.

Zhang, M. & Wen, L., 2013. High-precision location and yield of North Korea's 2013 nuclear test, *Geophys. Res. Lett.,* **40,** doi:10.1002/grl.50607.